

Long-Range Dependence in Financial Markets: Empirical Evidence and Generative Modeling Challenges

Yifan He^{*1} and Svetlozar Rachev¹

¹Department of Mathematics and Statistics, Texas Tech University, Lubbock, TX 79409, USA

September 25, 2025

Abstract

This study presents a comprehensive empirical investigation of the presence of long-range dependence (LRD) in the dynamics of major U.S. stock market indexes—S&P 500, Dow Jones, and Nasdaq—at daily, weekly, and monthly frequencies. We employ three distinct methods: the classical rescaled range (R/S) analysis, the more robust detrended fluctuation analysis (DFA), and a sophisticated ARFIMA–FIGARCH model with Student’s t -distributed innovations. Our results confirm the presence of LRD, primarily driven by long memory in volatility rather than in the mean returns. Building on these findings, we explore the capability of a modern deep learning approach, Quant generative adversarial networks (GANs), to learn and replicate the LRD observed in the empirical data. While Quant GANs effectively capture heavy-tailed distributions and some aspects of volatility clustering, they suffer from significant limitations in reproducing the LRD, particularly at higher frequencies. This work highlights the challenges and opportunities in using data-driven models for generating realistic financial time series that preserve complex temporal dependencies.

Keywords: Long-range dependence; rescaled range analysis; detrended fluctuation analysis; ARFIMA–FIGARCH model; Quant GANs

1 Introduction

The concept of long-range dependence (LRD), characterized by a slow, hyperbolic decay of the autocorrelations, signifies a persistent memory effect in a stochastic process where past events have a lasting influence on the future. This was first systematically studied by Hurst in the context of hydrology, where he observed persistent cycles in the long-term storage capacity of the Nile River reservoirs (Hurst, 1951). Mandelbrot and Wallis (1968) later formalized Hurst’s method into the rescaled range (R/S) analysis, bringing the concept into the realm of statistical physics and economics. Since then, the study of LRD has transcended disciplinary boundaries, finding applications in geophysics, network traffic analysis, and, notably, financial econometrics (Doukhan et al., 2002; Beran, 2017). In financial markets, the presence of LRD in asset returns or volatility contradicts the efficient market hypothesis’s weak form and has profound implications for risk

^{*}Correspondence: Yifan.He@ttu.edu

management, option pricing, and forecasting, as it suggests that shocks may have persistent, long-lasting effects (Lo, 1991).

Parallel to the development of the measurement of LRD, the field of machine learning has witnessed revolutionary advances in generative modeling. Among these, generative adversarial networks (GANs), introduced by Goodfellow et al. (2014), have emerged as a powerful framework for learning and replicating complex data distributions. GANs train a generator and a discriminator in an adversarial game, resulting in a generator capable of producing highly realistic synthetic data. This was specifically harnessed for financial data by Wiese et al. (2020), who proposed Quant GANs. Using a temporal convolutional network (TCN) architecture (Bai et al., 2018), Quant GANs are designed to generate synthetic financial time series that capture key stylized facts such as the volatility clustering and the non-normal, heavy-tailed distributions of the returns.

This rapid progress in deep generative models naturally leads to an important and unexplored question: can these sophisticated data-driven models, specifically Quant GANs, also learn and replicate the LRD inherent in financial time series? While Quant GANs are adept at capturing distributional properties and short-term volatility dynamics, their ability to model the slow decay of autocorrelations—a hallmark of LRD—remains an open empirical question. This gap in the literature has motivated our study.

This paper seeks to address this gap by first rigorously establishing the presence of LRD in the empirical data and then critically evaluating the ability of Quant GANs to learn this property. Section 2 describes the data, consisting of three major U.S. indexes (S&P 500, Dow Jones, and Nasdaq) at daily, weekly, and monthly frequencies, and demonstrates their pronounced deviation from normality. Section 3 measures LRD using three methods: R/S analysis, detrended fluctuation analysis (DFA), and a combined ARFIMA–FIGARCH model, confirming that LRD is a robust feature of the data, mainly in the volatility. By comparing the statistical properties of thousands of simulated paths against the empirical series, Section 4 investigates whether Quant GANs can learn these characteristics of the LRD. Finally, Section 5 concludes by summarizing our findings and discussing their implications for financial modeling and machine learning.

2 The Data

In this part, we describe the datasets used in this study. Section 2.1 introduces the three daily benchmark indexes of the U.S. stock market—S&P 500, Dow Jones, and Nasdaq—along with the corresponding time spans of the datasets. Based on the original data, we further construct two additional datasets with *weekly* and *monthly* frequencies through downsampling. Section 2.2 analyzes the *log-returns* of the three indexes and demonstrates, using multiple methods, that the distributions of the returns deviate from normality. This finding motivates the use of heavy-tailed error distributions, such as Student’s *t*-distribution, in the ARFIMA–FIGARCH modeling discussed in Section 3.3.

2.1 Three Benchmark Indexes of the U.S. Stock Market

The original dataset used in this study consists of the daily closing values of three benchmark indexes of the U.S. stock market—S&P 500, Dow Jones, and Nasdaq—covering the period from January 2, 1992, to December 30, 2024, for a total of 8310 trading days, retrieved using the `yfinance`¹ package in Python, with Yahoo Finance² serving as the data source. By downsampling the original dataset, we also obtain the weekly and

¹See <https://pypi.org/project/yfinance/>.

²Official website: <https://finance.yahoo.com/>.

monthly closing values of the three benchmark indexes, resulting in 1723 and 396 observations, respectively.

Figure 1 illustrates the daily price trajectories of these three benchmark indexes from January 2, 1992, to December 30, 2024, assuming an initial investment of \$1. It is evident that the overall trends of the three

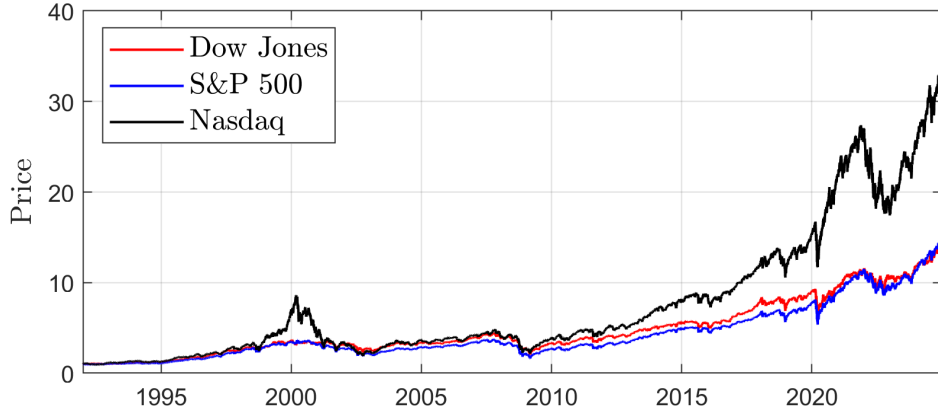


Figure 1: Daily price trajectories of the three benchmark indexes, assuming an initial investment of \$1 on January 2, 1992

indexes are upward over the entire period. Specifically, the trajectories of the S&P 500 and Dow Jones are very similar over the whole of the time span. The Nasdaq exhibits a pattern comparable to the S&P 500 and Dow Jones before 1998 and reaches its first significant peak around 2000. From 2001 to 2009, the three indexes display similar dynamics again. However, after 2009, the growth rate of the Nasdaq surpasses those of the S&P 500 and Dow Jones by a considerable margin. By the end of the sample period, the value of the Nasdaq is approximately three times higher than that of the S&P 500 and Dow Jones.

For simplicity, the weekly and monthly price trajectories of the three benchmark indexes are not presented.

2.2 The Non-Normal Nature of the Returns

In Section 2.1, we briefly examined the daily price time series of the three benchmark indexes. A subsequent discussion of their returns naturally follows.

There are two commonly used types of returns. The first is the *arithmetic return*, also referred to as the *simple return*:

$$R_t := \frac{P_t - P_{t-1}}{P_{t-1}} = \frac{P_t}{P_{t-1}} - 1,$$

where P_t denotes the asset's price at time t and R_t denotes the corresponding arithmetic return. The second type is the *logarithmic return* (or *log-return*), defined by

$$r_t := \ln \left(\frac{P_t}{P_{t-1}} \right) = \ln P_t - \ln P_{t-1},$$

where r_t denotes the log-return at time t .

Log-returns are often preferred in quantitative finance for several reasons. First, they are time-additive, meaning that the log-return over multiple periods equals the sum of the log-returns of the individual periods, which simplifies the modeling and analysis (Tsay, 2014). Second, log-returns approximate continuously compounded returns, making them more consistent with many financial models (Chambers et al., 2015; Butler, 2016). Lastly, they tend to better handle large price fluctuations and are more suitable for statistical

analysis under the assumption of normally distributed returns. In this study, unless otherwise specified, *all returns refer to log-returns*.

Figure 2 displays the daily³ returns of the three benchmark indexes. Across the three panels, we first observe that the returns of all three indexes fluctuate around zero, with values generally ranging from -0.15 to 0.15 . Moreover, the return series exhibit a clear volatility clustering pattern—periods of low volatility are typically followed by low volatility, while periods of high volatility are often followed by high volatility. This phenomenon, first documented by Mandelbrot et al. (1963) and later emphasized by Fama (1965), is a well-known stylized fact of financial time series.

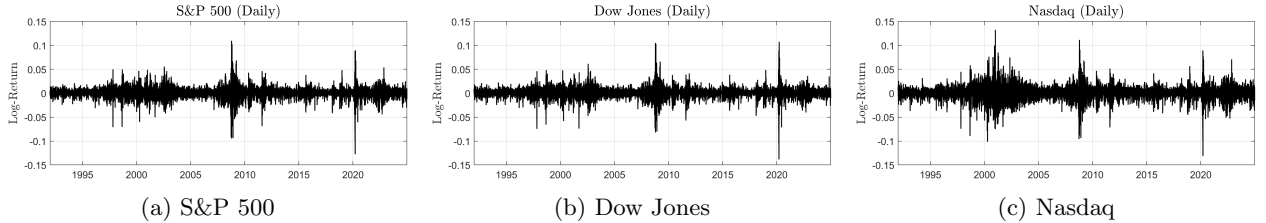


Figure 2: Daily returns of the three benchmark indexes

To better analyze the returns, we examine their distributions. Figure 3 presents the distributional characteristics of each benchmark index at a daily frequency. Each panel consists of two sub-panels: the left sub-panel displays the histogram of returns, overlaid with the kernel density estimate (blue solid line) and the fitted normal density (red dashed line), while the right sub-panel shows the corresponding quantile–quantile (QQ) plot. From the left sub-panels, it is evident that the return distributions deviate significantly from normality. Consistently, the QQ plots on the right reveal pronounced *fat-tailed behavior*⁴, as the sample quantiles deviate substantially from the red dashed reference line, with many observations lying far above and below it.

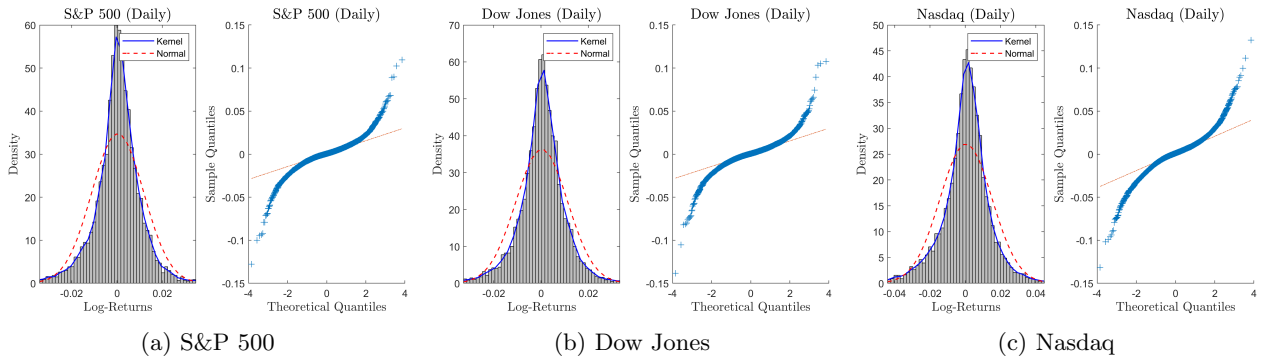


Figure 3: Histograms, kernel density estimates, normal density fits, and QQ plots of the daily returns for the three benchmark indexes

A normal distribution has skewness $\gamma = 0$ and kurtosis $\kappa = 3$. The difference $\kappa - 3$ is known as the *excess kurtosis*. Hypothesis tests are commonly used to assess deviations from normality arising from skewness, excess kurtosis, or both jointly (D'Agostino et al., 1990). In this study, we employ the `skewtest()`, `kurtosistest()`, and `normaltest()` functions from the `scipy.stats` Python subpackage to conduct these

³All corresponding figures for weekly and monthly returns are provided in Appendix A without explanatory texts.

⁴Fat-tailed distributions exhibit large negative and positive values with greater probability than a normal distribution.

respective tests. In each case, the null hypothesis assumes that the examined moments are consistent with those of a normal distribution.

Frequency	Index	γ^a	$\kappa - 3^a$
Daily	S&P 500	-0.410	10.9
	Dow Jones	-0.408	13.0
	Nasdaq	-0.207	6.51
Weekly	S&P 500	-0.821	7.25
	Dow Jones	-0.987	9.38
	Nasdaq	-0.889	7.53
Monthly	S&P 500	-0.779	1.51
	Dow Jones	-0.646	1.53
	Nasdaq	-0.733	2.04

^a All skewness and kurtosis p -values are less than 0.001.

Table 1: The results of the test for normality on the skewness γ and excess kurtosis $\kappa - 3$ for each benchmark index at different frequencies

Table 1 presents the results of the individual skewness and kurtosis tests for different return frequencies. For all cases, the null hypotheses are rejected at the 0.001 significance level. Consequently, the joint skewness–kurtosis test also rejects the null hypothesis of normality at the 0.001 level for all benchmarks and frequencies.

Combining the evidence from the QQ plots and hypothesis tests on the central moments, we find strong empirical support for rejecting the assumption of normally distributed returns for all three benchmark indexes, for all frequencies. In every case, the distributions exhibit negative skewness and are leptokurtic (i.e., they display positive excess kurtosis). Given these findings, we adopt heavy-tailed error distributions—such as Student’s t -distribution—in the ARFIMA–FIGARCH modeling framework discussed in Section 3.3.

3 Measurement of Long-Range Dependence

In this part, we focus on the key concept of this work—LRD, which refers to the slow decay of autocorrelations over time in a stochastic process. The notion of LRD was first introduced by Hurst (1951) in the context of hydrology, where Hurst observed that the fluctuations of the Nile River levels exhibited a persistent memory effect over long horizons. Since then, the study of LRD has attracted considerable attention in various fields, including geophysics, network traffic modeling, and particularly financial econometrics. In financial markets, the presence of LRD in asset returns or volatility has significant implications for risk management, asset pricing, and forecasting, as it indicates that shocks may have persistent effects over extended time periods (Doukhan et al., 2002; Beran, 2017).

In Section 3.1, we first employ the classical R/S analysis, proposed by Hurst (1951) and later formalized by Mandelbrot and Wallis (1968). This technique estimates the Hurst exponent to characterize the degree of persistence in a time series. While R/S analysis has been widely used, it suffers from several limitations, including its sensitivity to nonstationarities, structural breaks, and short-term dependencies (Lo, 1991). These shortcomings often lead to biased estimates of the Hurst exponent, making it less reliable for complex financial data.

To address these issues, Section 3.2 adopts DFA, originally developed by Peng et al. (1994) in the context of DNA sequence analysis. DFA improves upon R/S analysis by systematically removing local trends within different time scales before measuring the scaling behavior of fluctuations. This makes DFA particularly

robust for nonstationary financial time series and allows a more accurate detection of LRD (Kantelhardt et al., 2001).

Finally, because financial returns typically exhibit not only long memory but also volatility clustering and heavy-tailed distributions, Section 3.3 employs a combined modeling framework based on the ARFIMA(1, d_m , 1)–FIGARCH(1, d_v , 1) process with Student’s t -distributed innovations. The ARFIMA component captures long-range dependence in the conditional mean (Granger and Joyeux, 1980), while the FIGARCH component accounts for long memory in volatility (Baillie et al., 1996). The use of Student’s t further accommodates the leptokurtic nature of financial returns (Bollerslev, 1987), making the model suitable for capturing key stylized facts in financial markets, as we explained in Section 2.2.

3.1 Rescaled Range Analysis

To measure LRD, we use the Hurst exponent (H), which was first proposed by Hurst (1951). For a time series, $H = 0.5$ indicates a memoryless or random process, such as white noise or a standard random walk, where past values provide no information about future dynamics. When $H < 0.5$, the series exhibits anti-persistent behavior, meaning that increases are likely to be followed by decreases and vice versa; such processes tend to be mean-reverting, and their autocorrelations decay rapidly, implying no LRD. In contrast, $H > 0.5$ indicates persistent behavior, where positive (or negative) deviations are more likely to be followed by deviations of the same sign. This persistence corresponds to slowly decaying autocorrelations over long horizons, which is the hallmark of LRD.

We first investigate how to calculate H by R/S analysis. Consider a time series $\{X_t\}_{t=1}^N$. To examine scaling behavior across different time horizons, we define a set of subsequence lengths (scales) by

$$n = \frac{N}{2}, \frac{N}{4}, \frac{N}{8}, \dots, \quad (1)$$

where the maximum scale is chosen in such a way that at least four non-overlapping subsequences are available for the estimation. In practice, we set

$$n = \left\lfloor \frac{N}{2^p} \right\rfloor, \quad p = 0, 1, \dots, \left\lfloor \log_2 \left(\frac{N}{4} \right) \right\rfloor, \quad (2)$$

which ensures a sequence of evenly spaced scales on a logarithmic axis. For each selected scale n , the dataset is divided into $K = \lfloor N/n \rfloor$ ⁵ non-overlapping blocks of length n .

For the k -th block, we compute the sample mean \bar{X}_k and the cumulative deviation from the mean, defined as

$$Y_{k,j} = \sum_{i=1}^j (X_{k,i} - \bar{X}_k), \quad j = 1, \dots, n.$$

The range R_k cumulative deviations within the block is given by

$$R_k = \max(Y_{k,1}, \dots, Y_{k,n}) - \min(Y_{k,1}, \dots, Y_{k,n}),$$

⁵ $a = \lfloor b \rfloor$ means a is an integer satisfying $a \leq b < a + 1$.

and the corresponding standard deviation is

$$S_k = \sqrt{\frac{1}{n} \sum_{i=1}^n (X_{k,i} - \bar{X}_k)^2}.$$

The rescaled range for the block is $(R/S)_k = R_k/S_k$. For each scale n , the overall statistic $(R/S)_n$ is then obtained by averaging over all blocks:

$$(R/S)_n = \frac{1}{K} \sum_{k=1}^K \frac{R_k}{S_k}.$$

Hurst (1951) found that the expected value of the rescaled range follows a power-law relationship with the subsequence length n :

$$\mathbb{E}[(R/S)_n] = c \cdot n^H,$$

where c is a constant and H is the Hurst exponent we mentioned at the beginning of this section. Taking natural logarithms on both sides yields

$$\ln(R/S)_n = \ln c + H \cdot \ln n, \quad (3)$$

which implies that H can be estimated as the slope of a linear regression of $\ln(R/S)_n$ on $\ln n$.

Table 2 presents the results of the R/S analysis. First, the R^2 values are all above 0.99, indicating that Equation (3) provides an excellent fit to the relationship between $\ln n$ and $\ln(R/S)_n$. For visualization purposes, Figure 4 illustrates the fitting performance for the daily return series. Second, based on the point estimates, all estimated H values are greater than 0.5, suggesting that the return time series exhibit LRD. Moreover, for each index, the estimated H increases as the sampling frequency decreases (i.e., from daily to monthly), implying stronger persistence at lower frequencies. Finally, considering the 95% confidence intervals (CIs) of the estimates and the p -values from the hypothesis tests $H_0 : H = 0.5$ versus $H_a : H > 0.5$, we conclude that all return series indeed exhibit statistically significant LRD according to the R/S analysis.

Frequency	Index	\hat{H}^a	R^2	95% CI
Daily	S&P 500	0.564	0.997	[0.543, 0.585]
	Dow Jones	0.552	0.996	[0.529, 0.576]
	Nasdaq	0.587	0.998	[0.567, 0.607]
Weekly	S&P 500	0.601	0.998	[0.574, 0.627]
	Dow Jones	0.571	0.997	[0.545, 0.597]
	Nasdaq	0.619	0.998	[0.591, 0.647]
Monthly	S&P 500	0.664	0.996	[0.618, 0.710]
	Dow Jones	0.621	0.996	[0.574, 0.668]
	Nasdaq	0.665	0.997	[0.624, 0.706]

^a All p -values for hypothesis test $H_0 : H = 0.5$ vs. $H_a : H > 0.5$ are less than 0.001.

Table 2: The results of rescaled range analysis

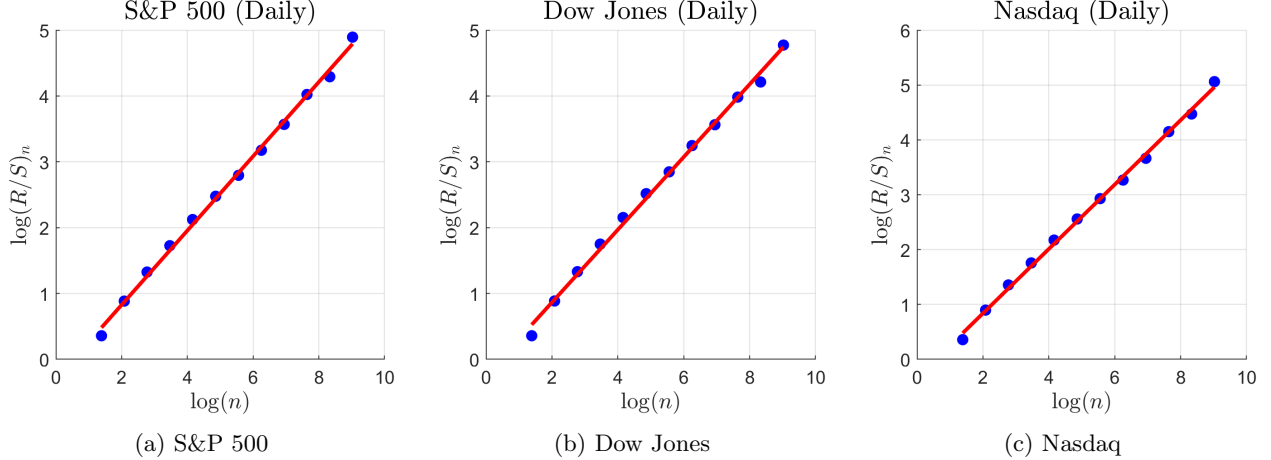


Figure 4: Rescaled range analysis for daily returns of the three benchmark indexes

3.2 Detrended Fluctuation Analysis

Section 3.1 used the R/S analysis to measure the LRD of the return time series, however, this classical method suffers from several limitations. First, the R/S statistic is highly sensitive to short-range correlations and nonstationarities in the data, which can lead to an upward bias in estimating the Hurst exponent (Mandelbrot and Wallis, 1968). Moreover, R/S analysis assumes that the underlying process is stationary, making it less robust when dealing with financial time series that often exhibit trends, volatility clustering, and structural breaks (Weron, 2002).

To overcome these shortcomings, we now employ DFA, which has been shown to provide a more reliable estimation of LRD by systematically removing local trends before calculating fluctuations, thereby mitigating the influence of nonstationarity (Peng et al., 1994; Kantelhardt et al., 2001). In particular, DFA can effectively distinguish between true long-range correlations and apparent scaling behavior caused by underlying trends or heteroskedasticity, which makes it especially suitable for analyzing financial return series (Barunik and Kristoufek, 2010).

The initial preparations for DFA are the same as Equations (1) and (2), i.e., we select a logarithmically spaced set of scales n and, for each n , partition the series $\{X_t\}_{t=1}^N$ into $K = \lfloor N/n \rfloor$ non-overlapping blocks of length n . We then form the mean-adjusted cumulative profile $Y(i) = \sum_{t=1}^i (X_t - \bar{X})$ for $i = 1, \dots, N$. Within each block $v = 1, \dots, K$, with local index $i = 1, \dots, n$, we fit a least-squares linear trend to the profile, $\hat{Y}_v(i) = a_v i + b_v$, where the (a_v, b_v) satisfy

$$(a_v, b_v) = \arg \min_{(a, b)} \frac{1}{n} \sum_{i=1}^n [Y((v-1)n + i) - (ai + b)]^2.$$

Let the corresponding residuals be $r_v(i) = Y((v-1)n + i) - \hat{Y}_v(i)$. The detrended root-mean-square fluctuation for block v at scale n is

$$F_v(n) = \sqrt{\frac{1}{n} \sum_{i=1}^n r_v(i)^2},$$

and the fluctuation function at scale n used in our estimation aggregates blocks by simple averaging,

$$F(n) = \frac{1}{K} \sum_{v=1}^K F_v(n).$$

Repeating this construction over all selected scales n yields pairs $(\ln n, \ln F(n))$. The Hurst exponent H is then obtained by ordinary least squares from the log–log scaling relation

$$\ln F(n) = H \cdot \ln n + C + \epsilon_n. \quad (4)$$

Table 3 presents the results of the DFA. First, the values of R^2 for all the return series are greater than 0.99, indicating that Equation (4) provides an excellent fit to the relation between $\ln n$ and $\ln F(n)$, similar to what we obtained between $\ln n$ and $\ln(R/S)_n$ using the R/S analysis. For the purposes of visualization, we display the fitting performance of the DFA in Figure 5 for the daily returns. However, it is evident that the Dow Jones index, across all three frequencies, does not exhibit significant LRD, whereas the S&P 500 and Nasdaq indices do. One possible explanation is that DFA, being more robust against non-stationarities and short-term trends than the traditional R/S analysis (Kantelhardt et al., 2001), mitigates the spurious detection of LRD; thus, the apparent LRD observed in the Dow Jones under R/S analysis is probably due to short-term correlations rather than true long-range dependencies.

Frequency	Index	\hat{H}	R^2	95% CI	p -Value ^a
Daily	S&P 500	0.516	0.998	[0.498, 0.534]	* ^b
	Dow Jones	0.498	0.997	[0.478, 0.519]	0.566
	Nasdaq	0.531	0.999	[0.518, 0.543]	*** ^c
Weekly	S&P 500	0.524	0.998	[0.502, 0.547]	*
	Dow Jones	0.489	0.994	[0.456, 0.522]	0.774
	Nasdaq	0.536	0.999	[0.522, 0.551]	***
Monthly	S&P 500	0.577	0.999	[0.557, 0.597]	***
	Dow Jones	0.529	0.995	[0.485, 0.573]	0.0746
	Nasdaq	0.560	0.997	[0.523, 0.596]	** ^d

^a The p -value is for hypothesis test $H_0 : H = 0.5$ vs. $H_a : H > 0.5$.

^b Indicates a p -value < 0.05 .

^c Indicates a p -value < 0.001 .

^d Indicates a p -value < 0.01 .

Table 3: The results of detrended fluctuation analysis

3.3 ARFIMA(1, d_m ,1)–FIGARCH(1, d_v ,1) with Student’s t -Distribution

In Sections 3.1 and 3.2, we provided analyses of the LRD by using R/S and the DFA method, respectively. While these non-parametric approaches effectively measure the presence of long-range dependence through the Hurst exponent, they do not explicitly model the dynamic structure of the returns or account for additional empirical features commonly observed in financial time series, such as volatility clustering and heavy-tailed distributions.

To address these limitations, this subsection employs a combined ARFIMA(1, d_m ,1)–FIGARCH(1, d_v ,1) framework with Student’s t -distributed innovations. In this setup, the ARFIMA component captures long-range dependence in the conditional mean (Granger and Joyeux, 1980), while the FIGARCH component

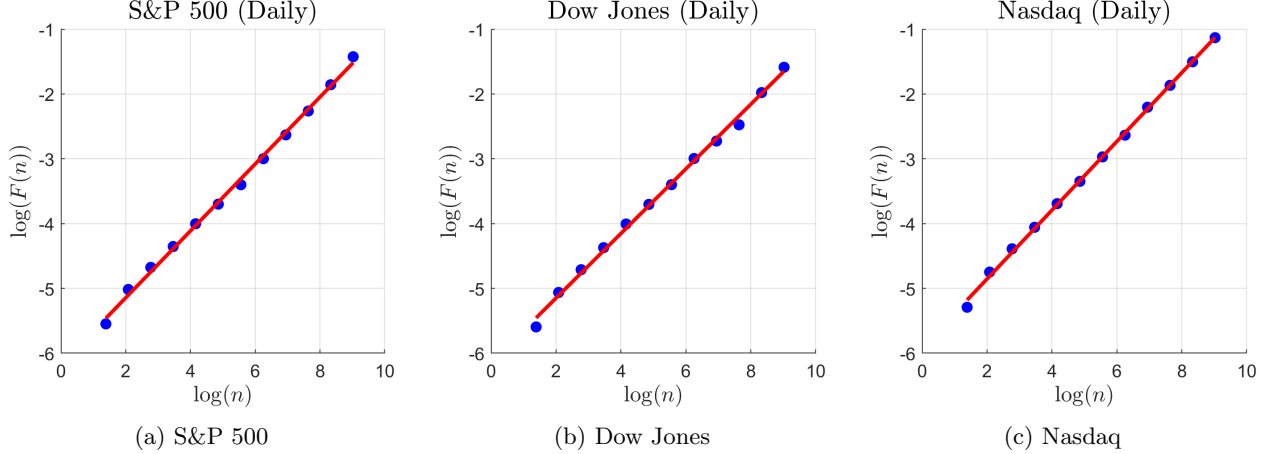


Figure 5: Detrended fluctuation analysis for daily returns of the three benchmark indexes

accounts for long memory in conditional volatility (Baillie et al., 1996). Student's t distribution further accommodates the leptokurtic nature of financial returns (Bollerslev, 1987), making the model suitable for capturing the key stylized facts in financial markets, as discussed in Section 2.2.

Given a time series $\{y_t\}$ (e.g., asset returns), suppose we have

$$\begin{aligned} y_t &= \mu_t + \epsilon_t, \\ \epsilon_t &= \sigma_t z_t, \end{aligned} \tag{5}$$

where

- $\mu_t = \mathbb{E}[y_t | \mathcal{F}_{t-1}]$ is the conditional mean (\mathcal{F}_{t-1} is the information we have up to time $t-1$),
- $\sigma_t^2 = \text{Var}[y_t | \mathcal{F}_{t-1}]$ is the conditional variance, and
- the z_t are the independently identical distributed residuals. In our case, we assumed the z_t follow Student's t distribution.

The structure of ARFIMA(p, d_m, q) is

$$\Phi_M(L)(1 - L)^{d_m}(y_t - \mu) = \Theta_M(L)\epsilon_t, \tag{6}$$

where

- $\mu = \mathbb{E}[y_t]$ is the unconditional mean,
- L is the lag operator (i.e., $Ly_t = y_{t-1}$),
- $\Phi_M(L) = 1 - \sum_{i=1}^p \phi_i L^i$,
- $\Theta_M(L) = 1 + \sum_{i=1}^q \theta_i L^i$, and
- $d_m \in (-0.5, 0.5)$ is the fractional differencing parameter for the mean.

The structure of FIGARCH(m, d_v, s) is

$$\Phi_V(L)(1 - L)^{d_v}\epsilon_t^2 = \omega + [1 - B_V(L)]\sigma^2, \tag{7}$$

where

- $\Phi_V(L) = 1 - \sum_{i=1}^m \alpha_i L^i$,
- $B_V(L) = \sum_{i=1}^s \beta_i L^i$,
- $d_v \in [0, 1]$ is the fractional differencing parameter for the volatility.

In our study, we combine Equations (5) through (7) and set $p = q = m = s = 1$ to obtain the ARFIMA(1, d_m , 1)–FIGARCH(1, d_v , 1) framework. Table 4 presents the result of fitting the ARFIMA–FIGARCH. For the conditional mean component (i.e., the ARFIMA part), all estimated d_m values are significantly greater than zero⁶, except for the daily returns of the Dow Jones index. Regarding the conditional volatility component (i.e., the FIGARCH part), an interesting finding emerges: all estimated d_v values are around 0.4 though their corresponding 95% CIs vary slightly. Combining the evidence from both d_m and d_v , we conclude that the returns of these three benchmarks, across different frequencies (with one exception, the Dow Jones at a daily frequency), exhibit LRD, which is primarily driven by their volatilities.

Frequency	Index	\hat{d}_m (p-Value ^a)	95% CI for \hat{d}_m	\hat{d}_v ^c	95% CI for \hat{d}_v
Daily	S&P 500	$7.95 \cdot 10^{-3}$ (***) ^b	$[7.82 \cdot 10^{-3}, 8.08 \cdot 10^{-3}]$	0.400	$[0.399, 0.401]$
	Dow Jones	$1.00 \cdot 10^{-8}$ (0.500)	$[-5.09 \cdot 10^{-5}, 5.10 \cdot 10^{-5}]$	0.400	$[0.397, 0.403]$
	Nasdaq	0.0383 (***)	$[0.0376, 0.0390]$	0.400	$[0.400, 0.401]$
Weekly	S&P 500	0.0725 (***)	$[0.0665, 0.0784]$	0.400	$[0.396, 0.404]$
	Dow Jones	0.0334 (***)	$[0.0332, 0.0337]$	0.400	$[0.399, 0.401]$
	Nasdaq	0.0190 (***)	$[0.0187, 0.0192]$	0.400	$[0.396, 0.404]$
Monthly	S&P 500	0.188 (***)	$[0.186, 0.190]$	0.400	$[0.399, 0.401]$
	Dow Jones	0.151 (***)	$[0.150, 0.151]$	0.400	$[0.397, 0.403]$
	Nasdaq	0.110 (***)	$[0.0965, 0.124]$	0.400	$[0.399, 0.401]$

^a The p -value is for hypothesis test $H_0 : d_m = 0$ vs. $H_a : d_m > 0$.

^b Indicates a p -value < 0.001 .

^c All p -values for hypothesis test $H_0 : d_v = 0$ vs. $H_a : d_v > 0$ are less than 0.0001.

Table 4: The results of ARFIMA–FIGARCH fit

4 Learning Long-Range Dependence in Financial Time Series

Section 3 introduced three methods for quantifying the LRD, enabling us to determine whether a return time series exhibits such dependence. Building upon these findings, we now turn to a related but distinct question: can the intrinsic LRD structure of financial returns be learned by modern data-driven approaches, particularly those based on machine learning and deep learning?

In this part, we investigate the potential of Quant GANs to replicate the LRDs observed in empirical return series. Section 4.1 provides a concise overview of the theoretical underpinnings of Quant GANs, originally developed by Wiese et al. (2020). As the primary objective of this work is not to conduct an in-depth algorithmic analysis, we limit our discussion to an intuitive explanation of the framework. Readers seeking a more comprehensive treatment are referred to the original paper and the corresponding implementation repository at <https://github.com/KseniaKingsep/quantgan>.

⁶We test whether d_m or d_v is significantly greater than zero because the fractional differencing parameter d is directly related to the Hurst exponent H via $H = d + 0.5$.

Subsequently, Section 4.2 evaluates the ability of Quant GANs to learn from return time series at different sampling frequencies. The empirical analysis contrasts synthetic data generated by Quant GANs with real financial data from multiple perspectives, including price dynamics and return distributions.

4.1 Quant GANs: Theoretical Framework

GANs were first introduced by Goodfellow et al. (2014) as a novel framework for generative modeling. A GAN consists of two neural networks, a *generator* G and a *discriminator* D , which are trained simultaneously in a two-player minimax game. The objective of the generator is to produce synthetic data samples that resemble the real data, while the discriminator aims to distinguish between the real and the generated samples. Formally, the original GAN optimization problem is expressed as

$$\min_G \max_D V(D, G) = \mathbb{E}_{x \sim p_{\text{data}}} [\log D(x)] + \mathbb{E}_{z \sim p_z} [\log(1 - D(G(z)))] \quad (8)$$

In Equation (8), $x \sim p_{\text{data}}$ means that x is sampled from the *true data distribution* p_{data} —for example, in a financial context, x could represent an observed historical return or price sequence—while $z \sim p_z$ means that z is sampled from a *prior noise distribution* p_z , typically chosen to be a simple Gaussian or uniform distribution. The generator G maps this noise z into a synthetic sample $G(z)$ intended to resemble real data. The discriminator D takes an input sample and outputs a scalar value $D(x) \in (0, 1)$, representing the estimated probability that the sample is real rather than generated.

The training process forms an adversarial game:

- The discriminator D maximizes $V(D, G)$ by improving its ability to correctly discriminate between real and generated data.
- The generator G minimizes $V(D, G)$ by learning to produce data $G(z)$ that the discriminator cannot distinguish from true data.

At equilibrium, the generator learns to approximate the true data distribution, i.e., $p_g \approx p_{\text{data}}$, resulting in synthetic samples that are statistically indistinguishable from real ones.

Building upon this framework, Quant GANs were proposed by Wiese et al. (2020) to address the challenges of the generation of synthetic financial time series. Unlike standard GANs, which focus purely on matching the overall data distribution, Quant GANs are designed to capture the domain-specific features observed in financial markets. Both the generator and discriminator are implemented using a TCN architecture, which is particularly effective for modeling sequential data with LRD.

Quant GANs serve as a simulation engine for financial markets. The generator G produces synthetic price or return sequences that replicate important statistical properties, such as volatility clustering, heavy-tailed distributions, and serial dependencies. The discriminator D acts as a quality controller, ensuring that the generated series are indistinguishable from real historical data. This makes Quant GANs very valuable in applications like stress testing, portfolio optimization, and derivative pricing, where large amounts of realistic yet synthetic financial data are needed.

4.2 Empirical Evaluation of Quant GANs

To evaluate the ability of Quant GANs to reproduce the statistical properties of financial time series, we adopt the implementation provided in the official repository: <https://github.com/KseniaKingsep/quantgan>.

The model is trained on historical return series using the default hyperparameter configuration described in the repository, including the TCN architecture for both the generator and the discriminator. After training, we generate 10000 synthetic paths of *log-prices* ($\ln P_t$) for each sampling frequency under consideration. The following analysis focuses exclusively on evaluating these simulated paths and contrasts them with the empirical data in terms of price dynamics, return distributions, and long-range dependence, without delving into the algorithmic details of the underlying model.

Displaying all 10000 simulated paths is impractical. For purposes of visualization, we randomly select 50 representative paths for each benchmark index. Figure 6 presents the simulated daily log-price paths. For

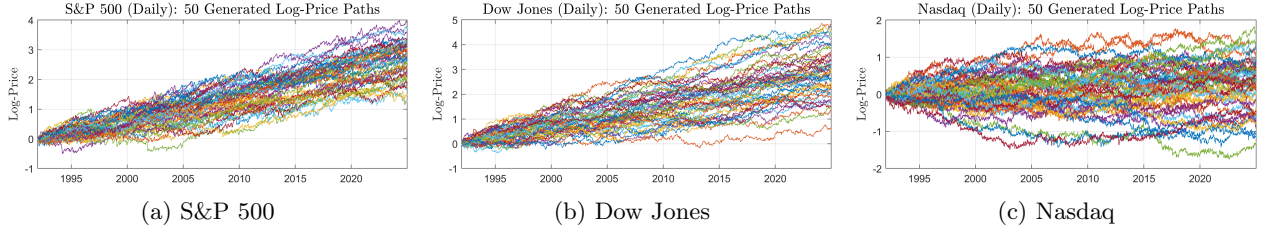


Figure 6: 50 randomly selected simulated daily log-price paths for the three benchmark indexes by Quant GANs

the S&P 500 and Dow Jones, most simulated paths exhibit an upward trend, whereas for the Nasdaq, while some paths show an increasing trend, others show a declining one.

To compare the empirical daily price series P_t^{real} with the price series simulated by Quant GANs P_t^{fake} , we select, among the 10000 generated paths, the one that minimizes the Euclidean distance to the empirical series:

$$\arg \min_i \|P_t^{\text{real}} - P_t^{\text{fake},i}\| = \arg \min_i \sqrt{\sum_{j=t_0}^{t_T} (P_j^{\text{real}} - P_j^{\text{fake},i})^2},$$

where $P_t^{\text{fake},i}$ denotes the i -th simulated path, and t_0 and t_T correspond to the start and end dates defined in Section 2.1, namely January 2, 1992, and December 30, 2024, respectively. The optimal index i naturally varies across benchmark indexes, as the path closest to the empirical series differs for each index. This path is used not only for the sake of visualization but also as the representative path in subsequent analyses, such as comparing return distributions and estimating the Hurst exponent or the fractional differencing parameter d . The rationale behind this choice is that the selected path best reflects the generative model's ability to replicate the historical price dynamics, making it the most informative candidate for further examination. Figure 7 compares the empirical (real) and simulated (fake) price series. For the S&P 500 and Dow Jones, the simulated paths closely follow the empirical trends over the entire sample period. In contrast, for the Nasdaq, even the optimal path fails to fully capture the sharp post-2020 growth observed in the empirical data.

To better compare the real and simulated price data, we examine their corresponding return distributions. Figure 8 illustrates the daily return distributions of both the real and simulated data. Although the simulated returns do not perfectly capture the concentration of real returns around zero, the left and right tails of the real return distribution are well modeled by the simulated data. This is particularly important in the context of risk management, where extreme gains and losses play a crucial role, and accurate modeling of tail behavior is essential (Danielsson and De Vries, 2000; Cont, 2001; Embrechts et al., 2013). Based on the visualization of price time series and the comparison of return distributions between real and simulated data, we conclude

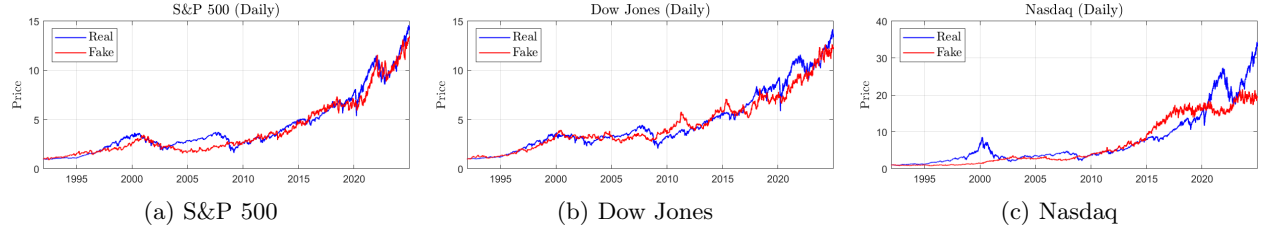


Figure 7: Empirical (blue) and simulated (red) daily price series for the three benchmark indexes

that the selected path generated by Quant GANs effectively captures the key statistical properties of the real data. Therefore, we proceed to apply the three methods introduced in Section 3 to further investigate the LRD of the simulated data.

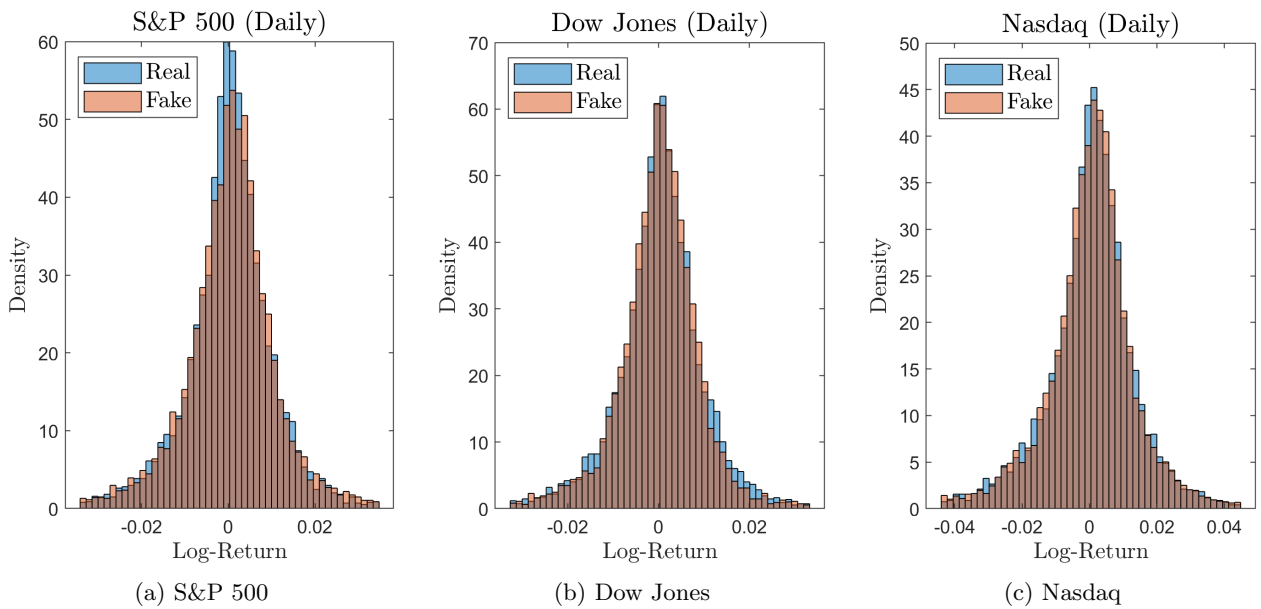


Figure 8: Comparison of empirical (blue) and simulated (orange) daily return distributions for the three benchmark indexes

Table 5 presents the results of R/S analysis of Quant GAN-generated data. First, the values of R^2 for all return series are around 99%, indicating that the estimates of the Hurst exponent obtained via linear regression are reliable. Second, compared with Table 2, we observe that at the daily frequency, the Hurst exponents of the empirical returns are all statistically greater than 0.5, indicating the presence of LRD. In contrast, for the Quant GAN-generated return series, LRD is not evident, as the p -values exceed 0.05, suggesting that the null hypothesis cannot be rejected. As the frequency decreases, the Dow Jones series exhibits LRD at weekly and monthly frequencies, and the Nasdaq series exhibits LRD at the monthly frequency. However, this may be due to the lower frequency, which tends to smooth out short-term fluctuations. In summary, we find that Quant GAN-generated data at a relatively high frequency (daily) fail to capture the LRD present in the empirical data.

Table 6 presents the DFA results for the data generated by Quant GANs. The values of R^2 of the linear regressions are consistently high across all return series (the lowest exceeding 96%), indicating that the Hurst exponents estimated using DFA are statistically reliable. A comparison between Tables 6 and 3 reveals a

Frequency	Index	\hat{H} (p-Value ^a)	R^2	95% CI
Daily	S&P 500	0.508 (0.335)	0.989	[0.469, 0.546]
	Dow Jones	0.519 (0.0583)	0.996	[0.494, 0.544]
	Nasdaq	0.490 (0.711)	0.997	[0.453, 0.523]
Weekly	S&P 500	0.492 (0.659)	0.990	[0.448, 0.536]
	Dow Jones	0.531 (* ^b)	0.997	[0.504, 0.557]
	Nasdaq	0.491 (0.707)	0.993	[0.454, 0.528]
Monthly	S&P 500	0.511 (0.290)	0.993	[0.462, 0.561]
	Dow Jones	0.555 (*)	0.994	[0.503, 0.606]
	Nasdaq	0.581 (*)	0.991	[0.519, 0.644]

^a The p -values are for hypothesis test $H_0 : H = 0.5$ vs. $H_a : H > 0.5$.

^b Indicates a p -value < 0.05 .

Table 5: The results of rescaled range analysis on Quant GAN-generated data

striking difference. For the empirical data (Table 3), six out of the nine return series exhibit LRD, while the Dow Jones series at all three frequencies do not. In contrast, the Quant GAN-generated data (Table 6) show no evidence of LRD across any of the nine series. Moreover, the corresponding p -values are substantially larger than 0.05, suggesting that we cannot reject the null hypothesis that the Hurst exponents equal 0.5. This discrepancy suggests that, at least under the DFA framework, the Quant GANs do not reproduce the LRD observed in the empirical data. However, this does not necessarily imply that the models are incapable of capturing LRD; rather, it may indicate that either DFA fails to detect LRD in the synthetic data, or the Quant GANs prioritize other statistical properties over LRD during generation. Further investigation using alternative measures of LRD would be necessary to draw a definitive conclusion.

Frequency	Index	\hat{H} (p-Value ^a)	R^2	95% CI
Daily	S&P 500	0.468 (0.921)	0.980	[0.421, 0.515]
	Dow Jones	0.472 (0.957)	0.991	[0.440, 0.505]
	Nasdaq	0.446 (0.986)	0.978	[0.399, 0.493]
Weekly	S&P 500	0.433 (0.976)	0.971	[0.366, 0.500]
	Dow Jones	0.451 (0.991)	0.991	[0.413, 0.489]
	Nasdaq	0.421 (0.985)	0.967	[0.351, 0.490]
Monthly	S&P 500	0.447 (0.876)	0.961	[0.344, 0.551]
	Dow Jones	0.433 (0.986)	0.987	[0.376, 0.489]
	Nasdaq	0.482 (0.663)	0.966	[0.377, 0.586]

^a The p -values are for hypothesis test $H_0 : H = 0.5$ vs. $H_a : H > 0.5$.

Table 6: The results of detrended fluctuation analysis on Quant GAN-generated data

Table 7 presents the ARFIMA–FIGARCH fit to the Quant GAN-generated data, in comparison with the results for the empirical data shown in Table 4. First, the estimated d_v is 0.4, indicating that the volatility exhibits LRD, characterized by clusters of high volatility followed by high volatility and clusters of low volatility followed by low volatility. Second, the estimated d_m for Quant GAN-generated data is statistically zero at the daily frequency for all three benchmark indices, whereas for the empirical data, only the Dow Jones shows d_m equal to zero. This suggests that Quant GANs fail to capture the LRD of daily returns for the S&P 500 and Nasdaq. At the weekly frequency, Quant GANs still do not capture the LRD of returns for the S&P 500 and Dow Jones, but they successfully capture it for the Nasdaq. At the monthly frequency, Quant GANs appear to capture the LRD of returns for all three indices, though this may be partly due to the lower frequency, which smooths short-term fluctuations and averages out trends. In summary, while

Quant GANs are effective at reproducing the LRD of volatility, they are less so at capturing the LRD of returns, particularly at higher (daily and weekly) frequencies. This highlights a limitation of the current Quant GAN framework in modeling the temporal dependence of asset returns.

Frequency	Index	\hat{d}_m (<i>p</i> -Value ^a)	95% CI for \hat{d}_m	\hat{d}_v ^c	95% CI for \hat{d}_v
Daily	S&P 500	$1.00 \cdot 10^{-8}$ (0.500)	$[-1.95 \cdot 10^{-4}, 1.95 \cdot 10^{-4}]$	0.400	[0.399, 0.401]
	Dow Jones	$1.00 \cdot 10^{-8}$ (0.500)	$[-7.25 \cdot 10^{-5}, 7.25 \cdot 10^{-5}]$	0.400	[0.399, 0.401]
	Nasdaq	$1.00 \cdot 10^{-8}$ (0.500)	$[-3.19 \cdot 10^{-5}, 3.19 \cdot 10^{-5}]$	0.400	[0.399, 0.401]
Weekly	S&P 500	$1.00 \cdot 10^{-8}$ (0.500)	$[-1.42 \cdot 10^{-4}, 1.42 \cdot 10^{-4}]$	0.400	[0.398, 0.402]
	Dow Jones	$1.00 \cdot 10^{-8}$ (0.500)	$[-7.09 \cdot 10^{-4}, 7.09 \cdot 10^{-4}]$	0.400	[0.399, 0.401]
	Nasdaq	0.0785 (***) ^b	[0.0782, 0.0787]	0.400	[0.399, 0.401]
Monthly	S&P 500	0.188 (***)	[0.186, 0.190]	0.400	[0.399, 0.401]
	Dow Jones	0.0352 (***)	[0.0350, 0.0355]	0.400	[0.398, 0.402]
	Nasdaq	0.0971 (***)	[0.0843, 0.109]	0.400	[0.396, 0.404]

^a The *p*-value is for hypothesis test $H_0 : d_m = 0$ vs. $H_a : d_m > 0$.

^b Indicates a *p*-value < 0.001 .

^c All *p*-values for hypothesis test $H_0 : d_v = 0$ vs. $H_a : d_v > 0$ are less than 0.0001.

Table 7: The results of ARFIMA-FIGARCH fit to Quant GAN-generated data

5 Conclusion

This study undertook a comprehensive empirical investigation into long-range dependence (LRD) in U.S. stock index returns and evaluated the capacity of Quant GANs to replicate this complex temporal dependency. Through a multi-method approach, we first robustly established the presence of LRD in the S&P 500, Dow Jones, and Nasdaq at daily, weekly, and monthly frequencies. The R/S analysis indicated significant persistence across all series. However, the more robust detrended fluctuation analysis revealed that this persistence in the Dow Jones was probably spurious, attributable to short-term correlations rather than genuine LRD. The ARFIMA-FIGARCH modeling provided the most nuanced insight, clearly indicating that the observed LRD is predominantly a feature of conditional volatility (captured by $d_v \approx 0.4$) rather than the conditional mean of returns.

The second part of our analysis demonstrated both the promise and the limitations of Quant GANs as a tool for financial time series generation. The model successfully generated synthetic paths that visually resembled empirical price trajectories and effectively captured the heavy-tailed, non-normal distribution of returns—a crucial aspect for risk management applications. However, a rigorous evaluation using the same battery of LRD tests revealed a significant shortcoming: the synthetic data generated by Quant GANs largely failed to replicate the LRD inherent in the original empirical series, particularly at daily and weekly frequencies. While the model replicated the LRD in the volatility (d_v), it did not consistently capture the LRD in the mean returns (d_m).

In conclusion, while Quant GANs constitute a significant advance in generative financial modeling, our findings suggest that their current architecture may prioritize learning distributional properties over complex long-memory dynamics. This indicates a critical area for future research. Enhancing the temporal convolutional network architecture or the adversarial training objective to explicitly account for long-range correlations could be a fruitful direction for developing next-generation models capable of fully replicating the intricate dependency structures of financial markets. Until then, practitioners should be cautious when using

such synthetic data for applications where long-term dependence is a critical factor, such as long-horizon forecasting or value-at-risk calculations.

References

Bai, S., Kolter, J. Z., and Koltun, V. (2018). An empirical evaluation of generic convolutional and recurrent networks for sequence modeling. *arXiv preprint arXiv:1803.01271*.

Baillie, R. T., Bollerslev, T., and Mikkelsen, H. O. (1996). Fractionally integrated generalized autoregressive conditional heteroskedasticity. *Journal of Econometrics*, 74(1):3–30.

Barunik, J. and Kristoufek, L. (2010). On Hurst exponent estimation under heavy-tailed distributions. *Physica A: Statistical Mechanics and its Applications*, 389(18):3844–3855.

Beran, J. (2017). *Statistics for Long-Memory Processes*. Routledge.

Bollerslev, T. (1987). A conditionally heteroskedastic time series model for speculative prices and rates of return. *The Review of Economics and Statistics*, pages 542–547.

Butler, K. C. (2016). *Multinational Finance: Evaluating the Opportunities, Costs, and Risks of Multinational Operations*. John Wiley & Sons.

Chambers, D. R., Anson, M. J., Black, K. H., and Kazemi, H. B. (2015). *Alternative Investments: CAIA Level I*. John Wiley & Sons.

Cont, R. (2001). Empirical properties of asset returns: Stylized facts and statistical issues. *Quantitative Finance*, 1(2):223.

D'Agostino, R. B., Belanger, A., and D'Agostino Jr., R. B. (1990). A suggestion for using powerful and informative tests of normality. *The American Statistician*, 44(4):316–321.

Danielsson, J. and De Vries, C. G. (2000). Value-at-Risk and extreme returns. *Annales d'Economie et de Statistique*, pages 239–270.

Doukhan, P., Oppenheim, G., and Taqqu, M. (2002). *Theory and Applications of Long-Range Dependence*. Springer-Verlag, Berlin.

Embrechts, P., Klüppelberg, C., and Mikosch, T. (2013). *Modelling Extremal Events: For Insurance and Finance*, volume 33. Springer-Verlag, Berlin.

Fama, E. F. (1965). The behavior of stock-market prices. *The Journal of Business*, 38(1):34–105.

Goodfellow, I. J., Pouget-Abadie, J., Mirza, M., Xu, B., Warde-Farley, D., Ozair, S., Courville, A., and Bengio, Y. (2014). Generative adversarial nets. *Advances in Neural Information Processing Systems*, 27:2672–2680.

Granger, C. W. and Joyeux, R. (1980). An introduction to long-memory time series models and fractional differencing. *Journal of Time Series Analysis*, 1(1):15–29.

Hurst, H. E. (1951). Long-term storage capacity of reservoirs. *Transactions of the American Society of Civil Engineers*, 116(1):770–799.

Kantelhardt, J. W., Koscielny-Bunde, E., Rego, H. H., Havlin, S., and Bunde, A. (2001). Detecting long-range correlations with detrended fluctuation analysis. *Physica A: Statistical Mechanics and its Applications*, 295(3-4):441–454.

Lo, A. W. (1991). Long-term memory in stock market prices. *Econometrica: Journal of the Econometric Society*, pages 1279–1313.

Mandelbrot, B. et al. (1963). The variation of certain speculative prices. *Journal of Business*, 36(4):394.

Mandelbrot, B. B. and Wallis, J. R. (1968). Noah, Joseph, and operational hydrology. *Water Resources Research*, 4(5):909–918.

Peng, C.-K., Buldyrev, S. V., Havlin, S., Simons, M., Stanley, H. E., and Goldberger, A. L. (1994). Mosaic organization of DNA nucleotides. *Physical Review E*, 49(2):1685.

Tsay, R. S. (2014). *An Introduction to Analysis of Financial Data with R*. John Wiley & Sons.

Weron, R. (2002). Estimating long-range dependence: Finite sample properties and confidence intervals. *Physica A: Statistical Mechanics and its Applications*, 312(1-2):285–299.

Wiese, M., Knobloch, R., Korn, R., and Kretschmer, P. (2020). Quant GANs: Deep generation of financial time series. *Quantitative Finance*, 20(9):1419–1440.

A Additional Figures

A.1 Log-Returns Time Series of Benchmark Indexes

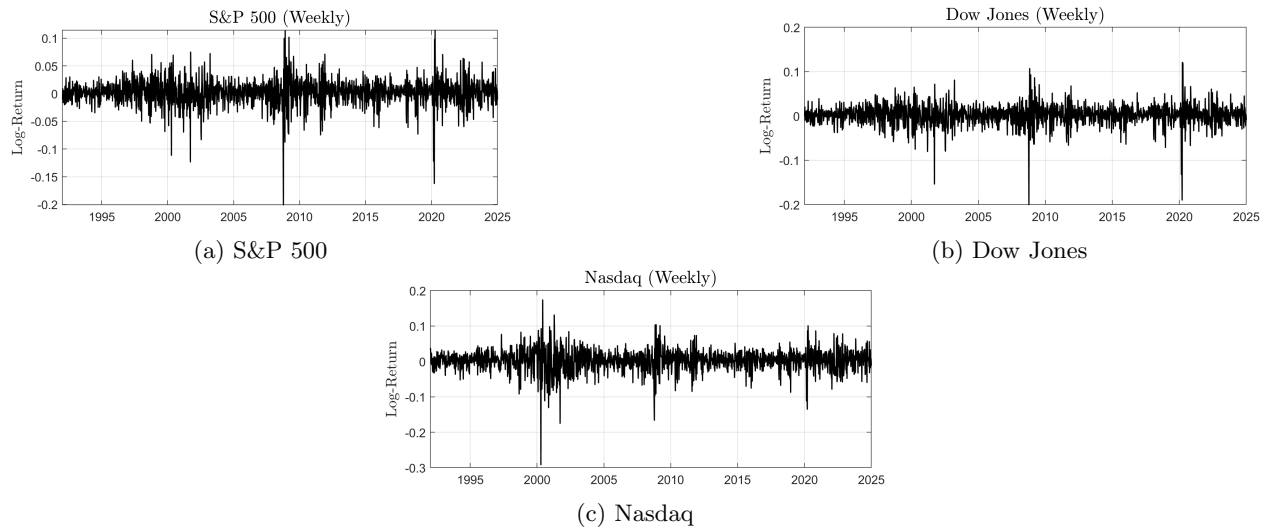


Figure 9: Weekly returns of the three benchmark indexes

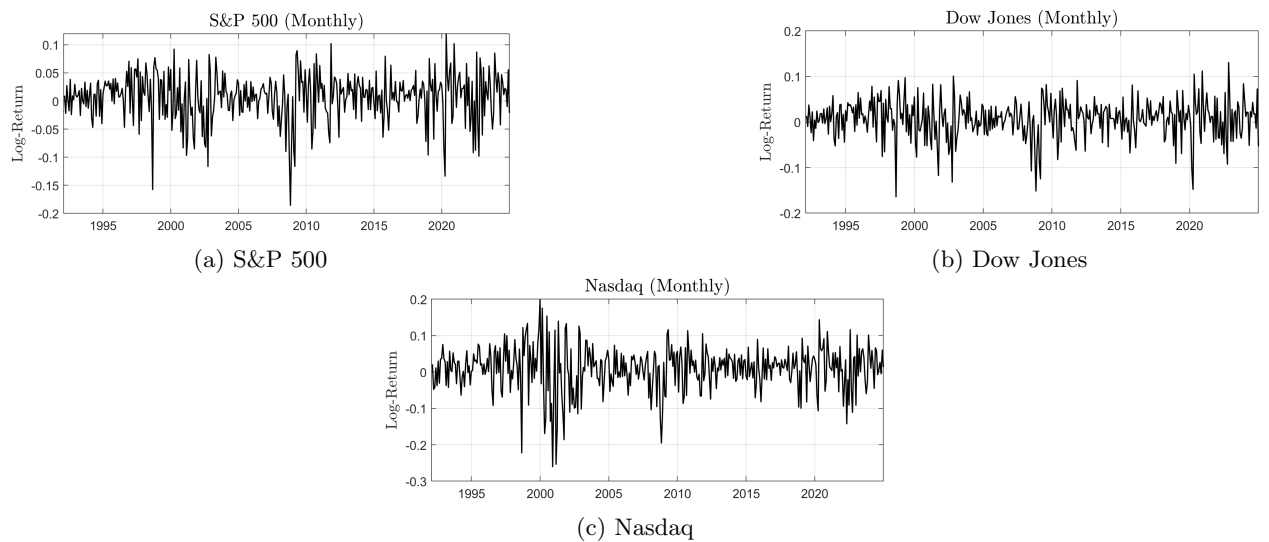


Figure 10: Monthly returns of the three benchmark indexes

A.2 Distributional Characteristics of Returns

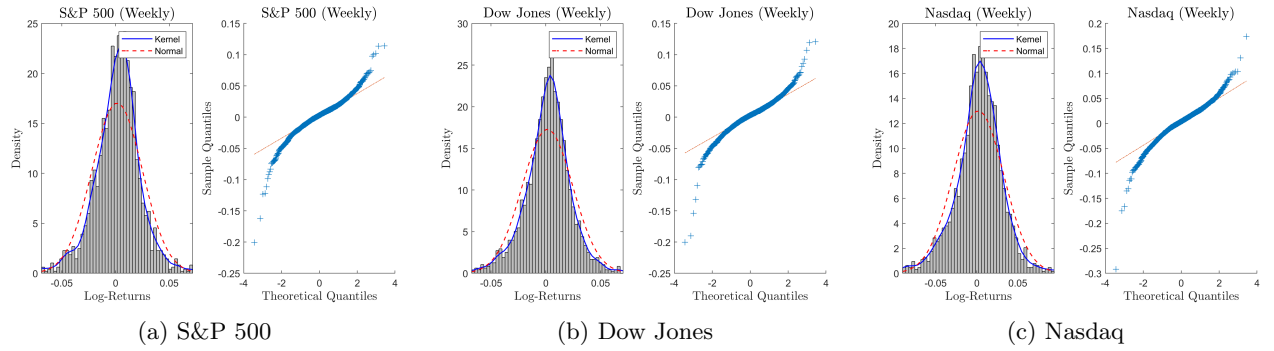


Figure 11: Histograms, kernel density estimates, normal density fits, and QQ plots of the weekly returns for the three benchmark indexes

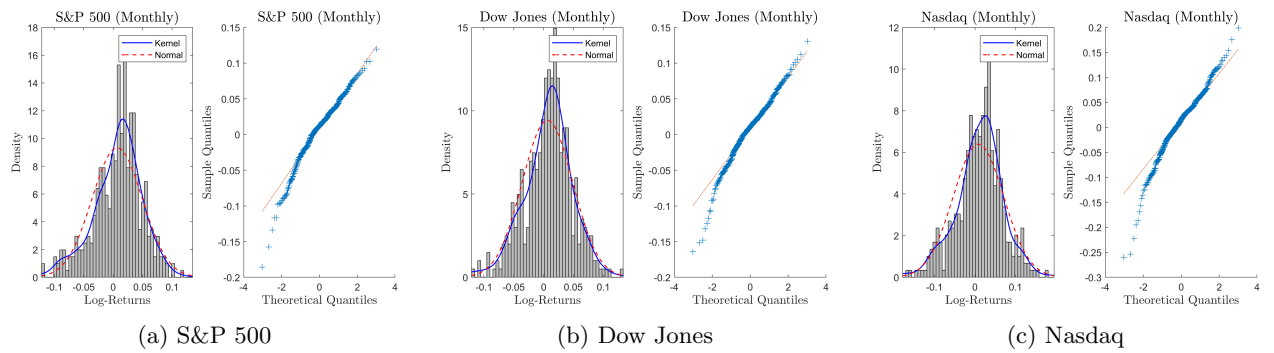


Figure 12: Histograms, kernel density estimates, normal density fits, and QQ plots of the monthly returns for the three benchmark indexes

A.3 Rescaled Range Analysis

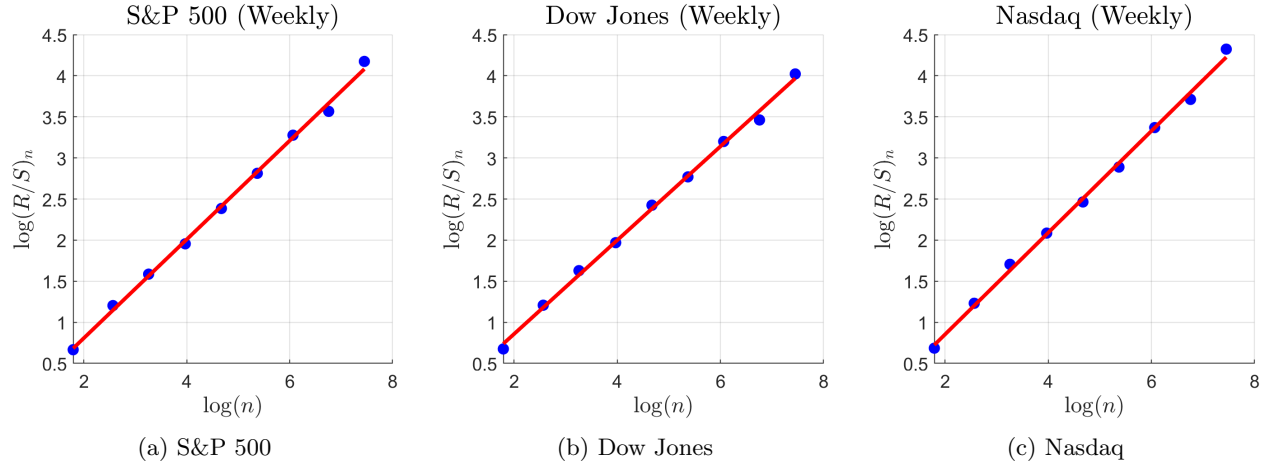


Figure 13: Rescaled range analysis for weekly returns of the three benchmark indexes

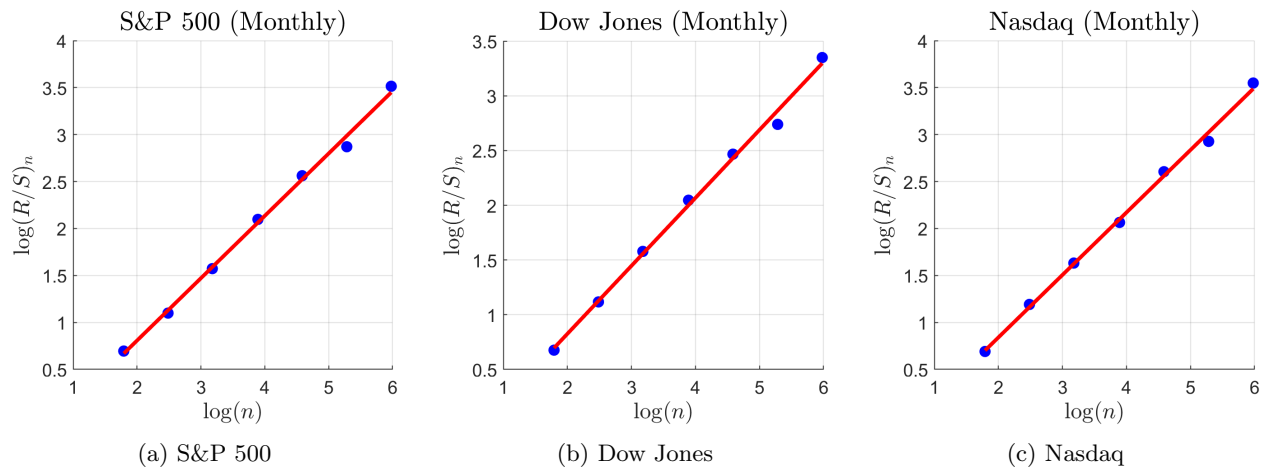


Figure 14: Rescaled range analysis for monthly returns of the three benchmark indexes

A.4 Detrended Fluctuation Analysis

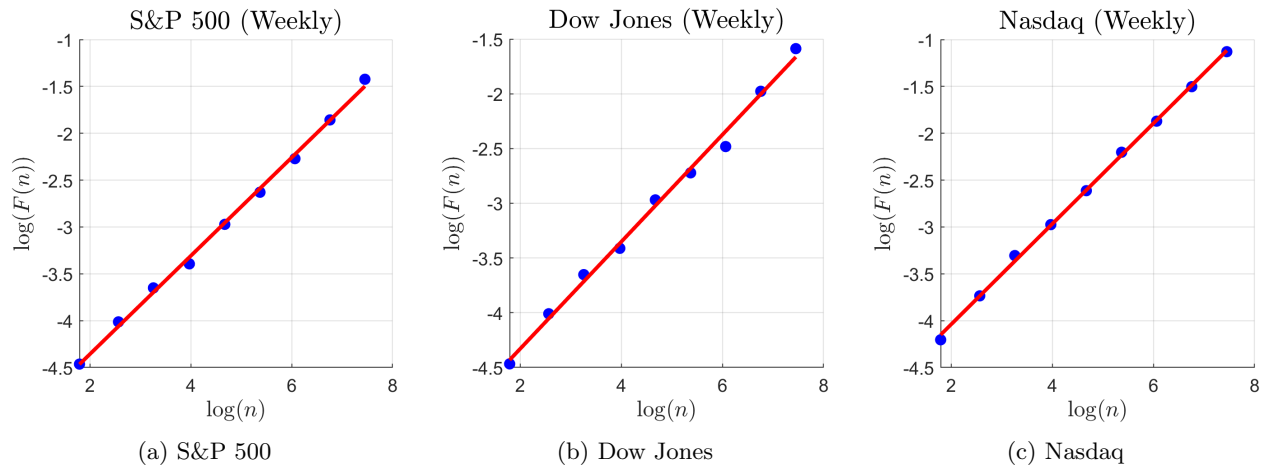


Figure 15: Detrended fluctuation analysis for weekly returns of the three benchmark indexes

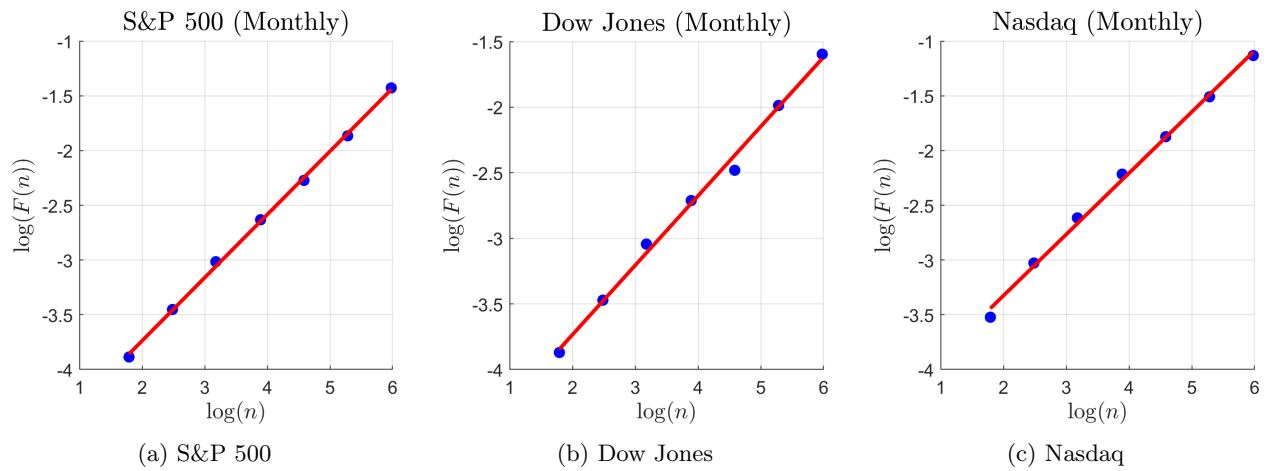


Figure 16: Detrended fluctuation analysis for monthly returns of the three benchmark indexes

A.5 Selected Simulated Log-Price Paths by Quant GANs

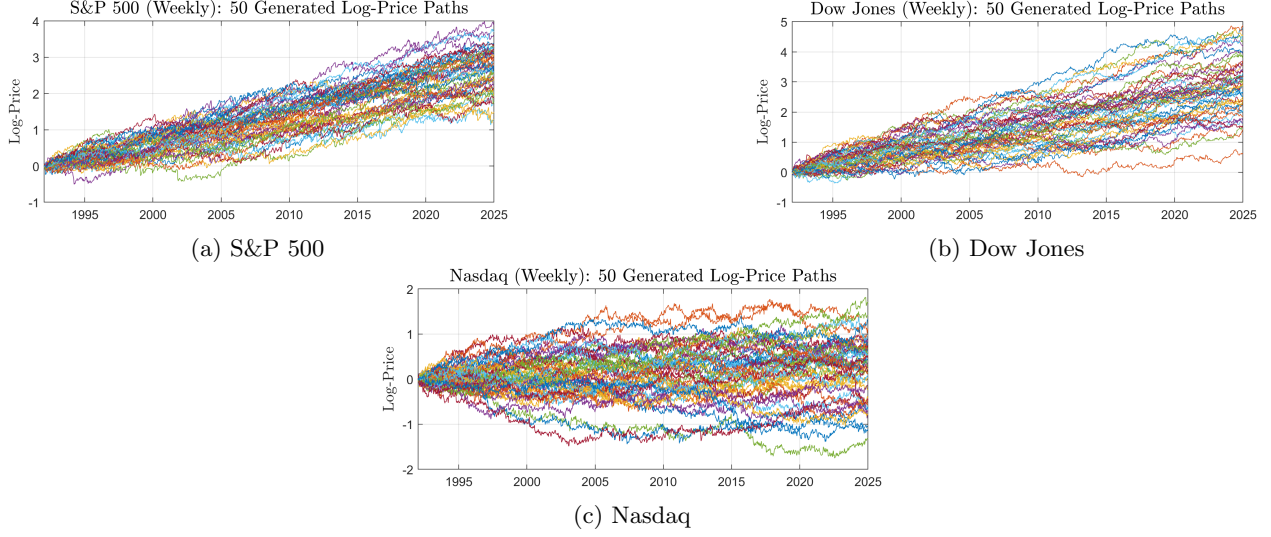


Figure 17: 50 randomly selected simulated weekly log-price paths for the three benchmark indexes by Quant GANs

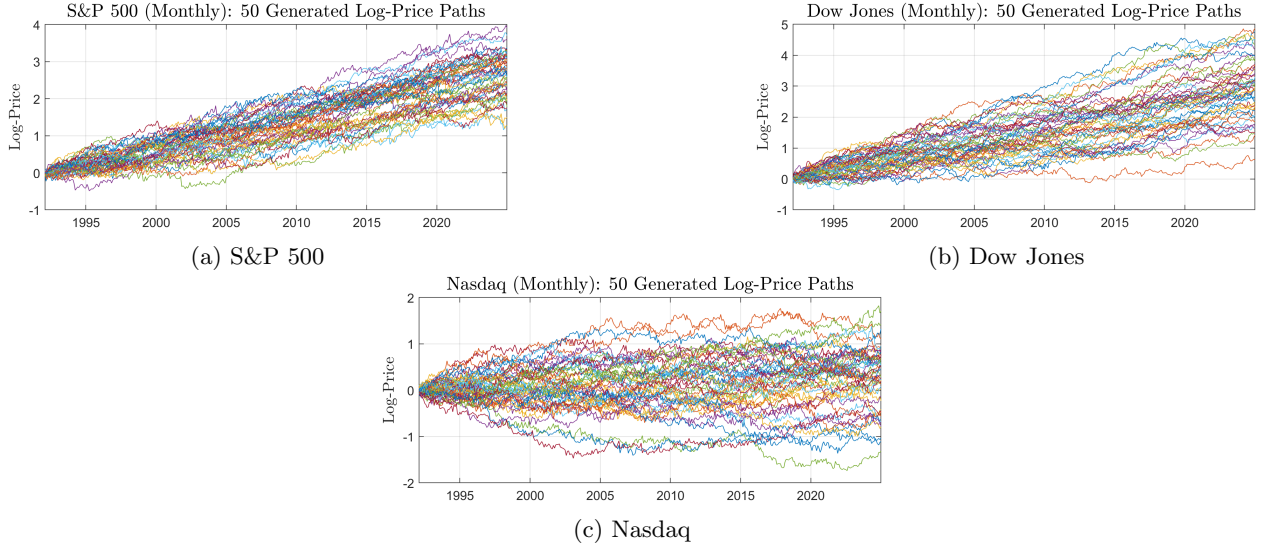


Figure 18: 50 randomly selected simulated monthly log-price paths for the three benchmark indexes by Quant GANs

A.6 Empirical and Quant GAN-Simulated Price Series

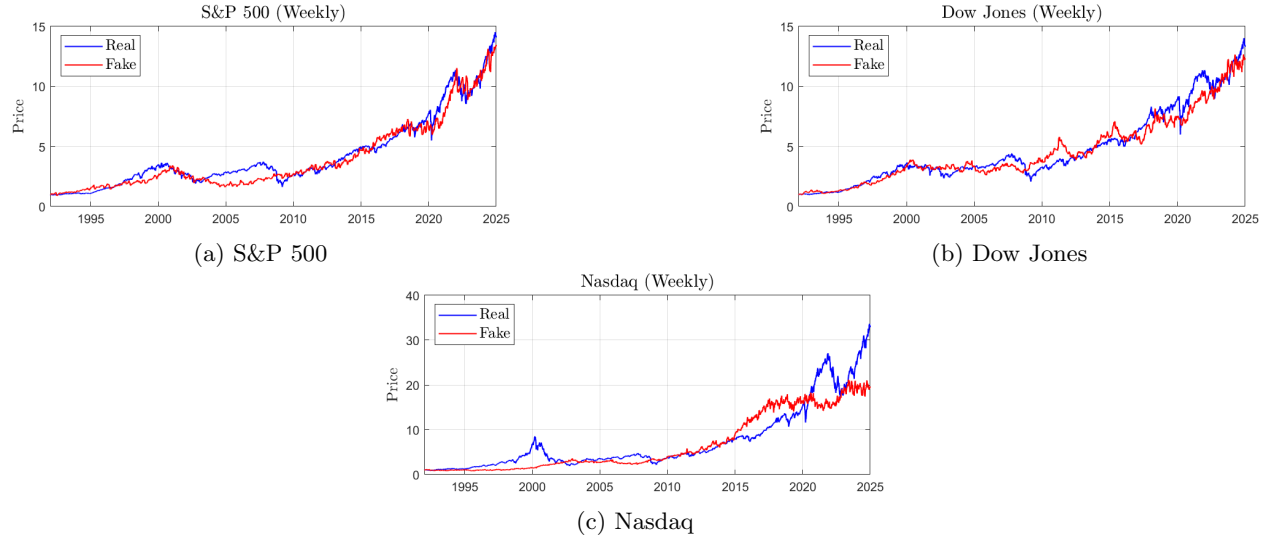


Figure 19: Empirical (blue) and simulated (red) weekly price series for the three benchmark indexes

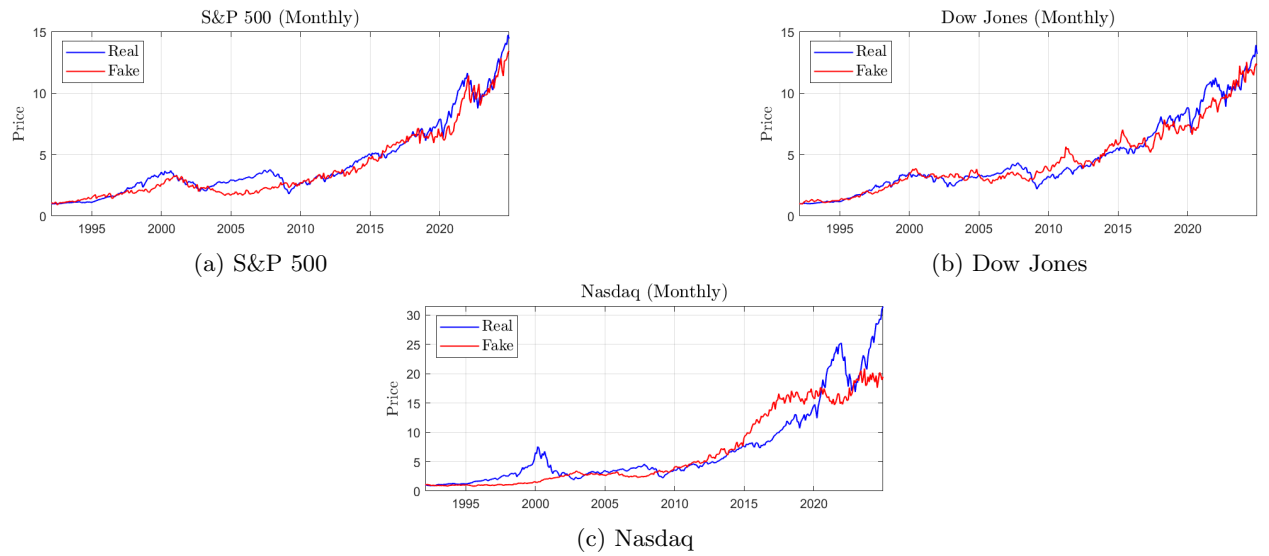


Figure 20: Empirical (blue) and simulated (red) monthly price series for the three benchmark indexes

A.7 Comparison of Empirical and Quant GAN-Simulated Return Distributions

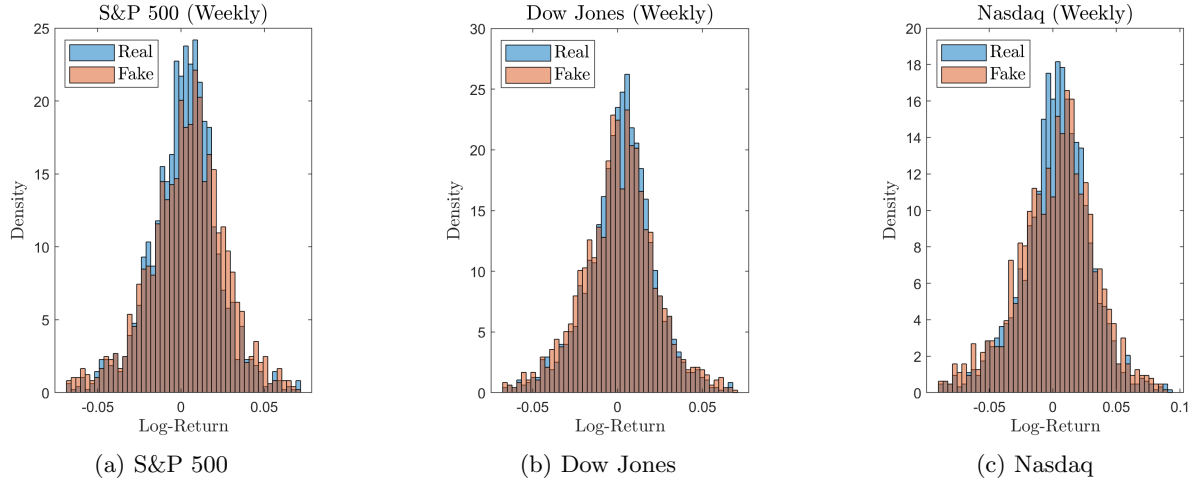


Figure 21: Comparison of empirical (blue) and simulated (orange) weekly return distributions for the three benchmark indexes

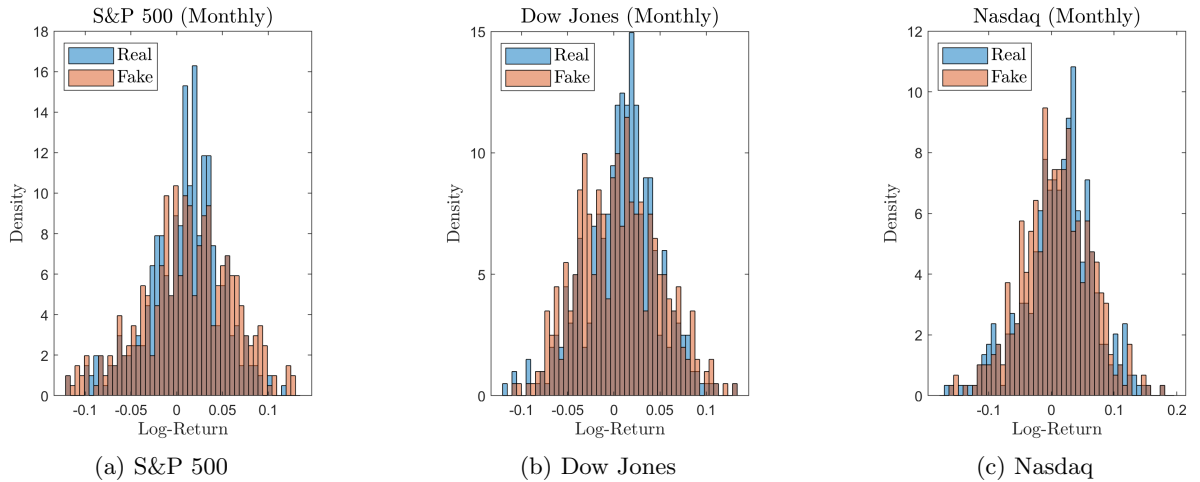


Figure 22: Comparison of empirical (blue) and simulated (orange) monthly return distributions for the three benchmark indexes